The University of Nottingham

UNITED KINGDOM · CHINA · MALAYSIA

Viel, Matteo and Haehnelt, Martin G. and Bolton, James S. and Kim, Tae-Sun and Puchwein, Ewald and Nasir, Fahad and Wakker, Bart P. (2017) Diagnosing galactic feedback with line broadening in the low redshift Lyα forest. Monthly Notices of the Royal Astronomical Society, 467 (1). L86-L90. ISSN 1365-2966

Access from the University of Nottingham repository:
http://eprints.nottingham.ac.uk/42519/8/slx004.pdf

Copyright and reuse:

A note on versions:

Diagnosing galactic feedback with line broadening in the low-redshift Lyα forest

Matteo Viel,[1,2,3]★ Martin G. Haehnelt,[4] James S. Bolton,[5] Tae-Sun Kim,[1] Ewald Puchwein,[4] Fahad Nasir[5] and Bart P. Wakker[6]

[1]*INAF – Osservatorio Astronomico di Trieste, Via G.B. Tiepolo 11, I-34131 Trieste, Italy*
[2]*SISSA, Via Bonomea 265, I-34136 Trieste, Italy*
[3]*INFN/National Institute for Nuclear Physics, Via Valerio 2, I-34127 Trieste, Italy*
[4]*Kavli Institute for Cosmology and Institute of Astronomy, Madingley Road, Cambridge CB3 0HA, UK*
[5]*School of Physics and Astronomy, University of Nottingham, University Park, Nottingham NG7 2RD, UK*
[6]*Department of Astronomy, University of Wisconsin–Madison, 475 N. Charter Street, Madison, WI 53706, USA*

ABSTRACT

We compare the low-redshift ($z \simeq 0.1$) Lyα forest from hydrodynamical simulations with data from the Cosmic Origins Spectrograph. We find the tension between the observed number of lines with b-parameters in the range of 25–45 km s^{-1} and the predictions from simulations that incorporate either vigorous feedback from active galactic nuclei or that exclude feedback altogether. The gas in these simulations is, respectively, either too hot to contribute to the Lyα absorption or too cold to produce the required linewidths. Matching the observed b-parameter distribution therefore requires feedback processes that thermally or turbulently broaden the absorption features without collisionally (over)ionizing hydrogen. This suggests that the Lyα forest b-parameter distribution is a valuable diagnostic of galactic feedback in the low-redshift Universe. We furthermore confirm that the low-redshift Lyα forest column density distribution is better reproduced by an ultraviolet background with the H I photoionization rate a factor of 1.5–3 higher than predicted by Haardt and Madau.

Key words: methods: numerical – intergalactic medium – quasars: absorption lines – diffuse radiation – large-scale structure of Universe.

1 INTRODUCTION

Lyα forest data have become an important tool in studying the physical state of the intermediate-redshift ($2 < z < 5$) intergalactic medium (IGM) and circumgalactic medium. With the advent of the Cosmic Origins Spectrograph (COS) on the *Hubble Space Telescope* (*HST*), it has become possible to obtain much improved measurements also at lower redshifts (Savage et al. 2014; Shull, Danforth & Tilton 2014; Danforth et al. 2016; Pachat et al. 2016; Werk et al. 2016). The increased resolution and signal-to-noise ratio (S/N) of the COS data enable the measurement of the column density of Lyα absorbers to lower values and help resolve the thermal broadening for weaker absorbers, complementing earlier investigations of the low-redshift IGM (Weymann et al. 1998; Janknecht et al. 2006; Kirkman et al. 2007).

Concurrently, the interpretation of these data has been aided by high dynamic range cosmological hydrodynamical simulations incorporating much of the relevant (subgrid) physics at $z = 0$

(Davé et al. 2010; Tornatore et al. 2010; Tepper-García et al. 2012; Ford et al. 2013; Rahmati et al. 2016; Villaescusa-Navarro et al. 2016). The present consensus on the nature of these absorbers is that they trace galactic environments relatively faithfully and may be used to address a wide set of scientific questions, from finding the missing baryons to the nature of the ultraviolet background (UVB) and galactic feedback. Here, we compare a new measurement of the observed H I Lyα Doppler b-parameter and column density distribution at $z = 0.1$ with predictions from a range of state-of-the-art numerical simulations. We assess whether constraints on the physical mechanism responsible for stellar and active galactic nuclei (AGN) feedback may be obtained, and revisit the possible missing ionizing photon problem first discussed by Kollmeier et al. (2014) and further investigated by Shull et al. (2015), Wakker et al. (2015), Khaire & Srianand (2015) and Gurvich, Burkhart & Bird (2016).

2 COS DATA

We have selected 44 *HST*/COS AGN spectra available as of 2015 December in the *HST* MAST (Mikulski Archive for Space Telescopes). The two main selection criteria are as follows: an S/N per

★ E-mail: viel@sissa.it

Table 1. Hydrodynamical simulations used in this work. The columns list the simulation name; the H I photoionization rate, Γ, in units of $10^{-12}\,\mathrm{s}^{-1}$; T_0, the median temperature at the mean density (log. units, volume weighted) calculated for a random sampling of gas at $\log(1+\delta) = [-0.1, 0.1]$ and excluding gas hotter than 10^5 K; T_+, the median temperature for overdensities $\delta = [4-40]$ (logarithmic units); the simulated mean transmitted flux; the rescaling factor A_f applied to match the CDDF in the range of $\log(N_{\mathrm{HI}}/\mathrm{cm}^{-2}) = [13-14]$; the mean flux obtained; and the new $\Gamma_f = \Gamma/A_f$ value inferred from the rescaling. Quantities are at $z = 0.1$. The observed mean flux is $\overline{F} = 0.983$ from Danforth et al. (2016).

Model	Γ	T_0	T_+	$\overline{F}$	A_f	$\overline{F}_f$	Γ_f
HM01	0.127	3.72	4.93	0.985	1.252	0.982	0.101
HM01$_{\mathrm{hot}}$	0.127	3.99	5.00	0.989	2.007	0.981	0.063
HM01$_{\mathrm{vhot}}$	0.127	4.08	5.00	0.990	2.426	0.980	0.052
HM12	0.035	3.71	4.90	0.964	0.408	0.981	0.087
HM12$_{\mathrm{hot}}$	0.035	3.97	4.94	0.972	0.624	0.981	0.057
Illustris	0.048	3.73	6.19	0.976	0.982	0.977	0.049
Sherwood	0.035	3.91	5.12	0.965	0.496	0.979	0.071

resolution element that is larger than 20 and an emission redshift in the redshift range of $0.1 < z < 0.35$, covering the Lyα forest at $0 < z < 0.2$. The first criterion was imposed so that the detection limit is $\log N_{\mathrm{HI}}/\mathrm{cm}^{-2} \sim 13$. The final co-added COS spectra have a resolution of $\sim$18–20 km s^{-1} in a heliocentric velocity frame and have S/N $\in [30-150]$ per resolution element in the Lyα forest region. The total redshift coverage is $\Delta z = 4.991$, excluding Milky Way interstellar medium line contamination and unobserved wavelength regions. Details of the COS data reduction and the properties of the AGN spectra can be found in Wakker et al. (2015) and Kim et al. (in preparation), respectively.

After initial continuum fitting, all the absorption profiles were identified and fitted with a Voigt profile using VPFIT (Carswell & Webb 2014) to obtain the column density and the b-parameter (see Kim et al. 2013, 2016, for more details). VPFIT is also used to obtain line parameters for our simulated spectra. Since the simulated spectra are fitted only with H I Lyα lines, we have also fitted the observed Lyα lines without using any higher order Lyman series lines. Depending on the date of the observation, a non-Gaussian COS line spread function (LSF) at the different lifetime positions was used (Kriss 2011). At $0 < z < 0.2$, the total number of fitted H I lines is 704 at $\log N_{\mathrm{HI}}/\mathrm{cm}^{-2} \in [12.5, 14.5]$, with the b-parameters spanning the range of 8–181 km s^{-1}. There are 424 lines with $\log N_{\mathrm{HI}}/\mathrm{cm}^{-2} \in [13, 14]$ with a relative error on the b-parameter smaller than 0.5: This will constitute our main sample. For comparison, we shall also use the Lyα lines obtained by Danforth et al. (2016) from 39 COS AGN ($\Delta z = 4.33$). We find a good agreement between the data set used here and the one presented in Danforth et al. (2016, hereafter D16), as will be demonstrated later.

3 NUMERICAL SIMULATIONS

We consider a range of state-of-the art Λ cold dark matter cosmological hydrodynamic simulations, including the Illustris (Vogelsberger et al. 2014; Nelson et al. 2015) and Sherwood (Bolton et al. 2017) simulations. The majority of the simulations have been performed with the parallel Tree-PM smoothed particle hydrodynamics (SPH) code P-GADGET-3 (Springel 2005), apart from Illustris, which was run with the moving-mesh code AREPO (Springel 2010). The simulations include a variety of star formation and stellar or AGN feedback implementations as well as a range of UVB models. We have also boosted the He II photoheating rates in some models in an ad hoc manner (as described in Bolton et al. 2008) to obtain temperatures for the low-density, photoionized IGM that better match the observed b-parameter distribution. The main properties of the individual simulations are as follows.

HM (Haardt & Madau UVB models): These are P-GADGET-3 simulations with a range of assumptions for the UVB and temperature of the low-density IGM. HM simulations are performed without feedback using a simplified star formation criterion that turns all gas particles with a density above $\rho/\langle\rho\rangle = 10^3$ and a temperature below 10^5 K into star particles. This feature is labelled QUICKLYA and was first used by Viel, Haehnelt & Springel (2004). The Haardt & Madau (2001, hereafter HM01) runs differ from the Haardt & Madau (2012, hereafter HM12) simulations in the choice of precomputed UVB model and hence H I photoionization rate, which is $\Gamma/(10^{-12}) = 0.035$ and 0.127 for HM01 and HM12, respectively (see Table 1). In addition, the thermal history for each simulation is labelled 'hot' or 'vhot', indicating a different assumption for the gas temperature, T_0, at the mean background density, which is in the range of $\log(T_0/K) = 3.7$–4.1. All the HM models are run with a linear box size of $60\,h^{-1}$ comoving Mpc and 2×512^3 gas and dark matter particles.

Illustris: The Illustris simulation has a linear box size of $75\,h^{-1}$ comoving Mpc and follows the evolution of 2×1820^3 gas cells and dark matter particles. The star formation and feedback model uses supernovae-driven winds that scale with the velocity dispersion of the host halo (Vogelsberger et al. 2013). AGN feedback is based on Sijacki et al. (2007) and uses two models – radiatively efficient and 'radio-mode' – depending on the black hole accretion rate. In the latter case, 7 per cent of the accreted rest mass energy is thermally injected into AGN bubbles. The individual injection events are highly energetic, corresponding to roughly $0.01M_{\mathrm{BH}}c^2$. Photoionization and heating are followed using the Faucher-Giguère et al. (2009) UVB, and self-shielding and ionizing flux from nearby AGN are accounted for. This results in $\Gamma/(10^{-12}) = 0.048$, $\log(T_0/K) = 3.7$ and a relatively high temperature for gas at moderate overdensities $\log(T_0/K) = 6.2$ (see Table 1).

Sherwood: The Sherwood simulation that we primarily use here was performed with a linear box size of $80\,h^{-1}$ comoving Mpc and 2×512^3 particles. It employs the star formation and feedback model described in Puchwein & Springel (2013). This follows the star formation prescription of Springel & Hernquist (2003) with a Chabrier initial mass function and supernovae-driven winds with velocities that scale with the escape velocity of the galaxy. The AGN feedback is again based on Sijacki et al. (2007) but with more modest assumptions about the available energy; 2 per cent of the accreted rest mass energy is injected in the radio mode, and individual events are much less energetic, with $\gtrsim 2 \times 10^{-6}M_{\mathrm{BH}}c^2$. In addition, two further Sherwood runs at different resolutions are used for convergence testing (not shown in any of the figures). These use the simpler QUICKLYA treatment, and have the same box size
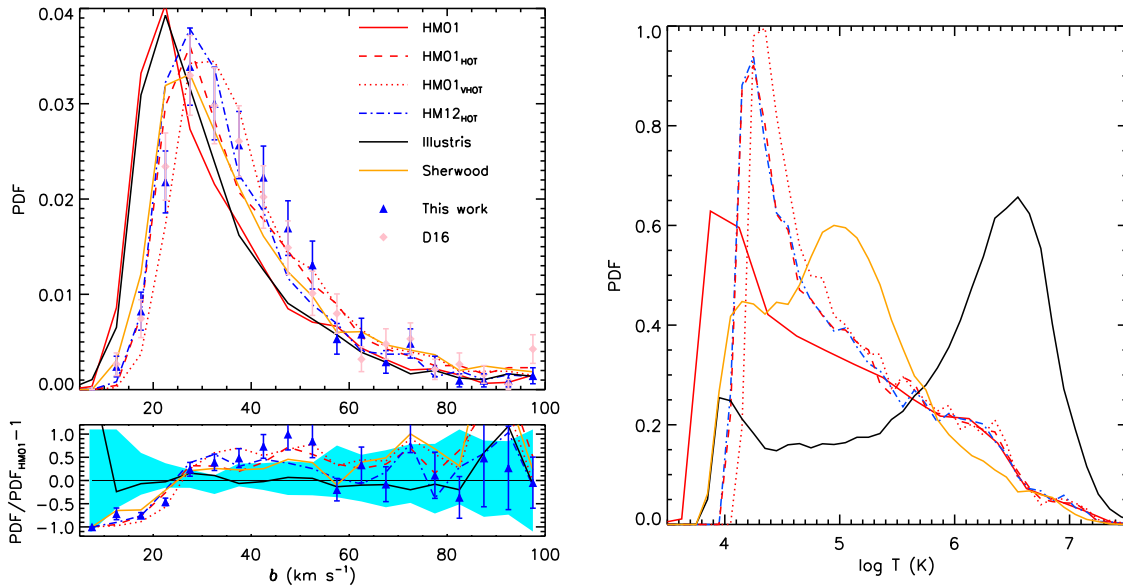
Figure 1. Left-hand panel: the *b*-parameter distribution for HM01 (red solid line); HM01$_{hot}$ (dashed red line); HM01$_{vhot}$ (dotted red line); HM12$_{hot}$ (blue dot–dashed line); Illustris (black solid line); and Sherwood (orange solid line). The bottom panel shows the ratio of the linewidth PDFs with respect to HM01. The shaded area indicates the $\pm 2\sigma$ range obtained from a set of 100 mocks with the same redshift path as the data. COS data are represented by the blue triangles (Poisson error bars), while the D16 data are shown as pink diamonds. The spectra have been scaled to match the observed CDDF at $N_{H I} = 10^{13}$–10^{14} cm^{-2}, and only lines with $N_{H I}/$cm$^{-2} = 10^{13}$–10^{14} and for which the relative error on the *b*-parameter is smaller than 0.5 are used for all data shown. Right-hand panel: distribution of the volume weighted gas temperature when selecting gas with overdensities in the range of $\delta = 4$–40.

of $80\,h^{-1}$ comoving Mpc and have 2×512^3 or 2×1024^3 particles, respectively. This run has $\Gamma/(10^{-12}) = 0.035$ and $\log(T_0/K) = 3.9$.

The cosmological parameters for all the simulations are in agreement with either Hinshaw et al. (2013) or Planck Collaboration XVI (2014). Simulated spectra are extracted from all models at $z = 0.1$ along 1000 random lines of sight (our results have converged for this number of spectra). Resolution effects are taken into account by convolution with the COS LSF. The S/N per resolution element is chosen to be 30. The simulated spectra are then analysed with VPFIT adapted for the deconvolution of the COS LSF, using the same procedure used to fit the observational data. Although we will show data for a wider range of column densities, it is only the range of $N_{H I} = 10^{13}$–10^{14} cm^{-2} that we found to be robust with regard to resolution and noise issues (we discuss this further below). Unless otherwise stated, we therefore scale the mean transmitted flux of the spectra to match the observed column density distribution function (CDDF) in this range. This rescaling is performed by modifying the optical depth in each pixel of the simulated spectra by a constant, A_f, such that $\overline{F}_f = \langle e^{-A_f \tau_i} \rangle$. Table 1 summarizes the simulations along with some quantities discussed in the following sections.

We have also performed a series of convergence checks on the simulations. With regard to mass resolution, when comparing the CDDFs of the QUICKLYA Sherwood runs (not shown in Table 1), we found an agreement at the 15 per cent level in the range of $\log(N_{HI}/$cm$^{-2}) = 12.5$–14.5, while the *b*-parameter distributions agree to within 20 per cent at > 20 km s^{-1}. Regarding box size effects, we found that the HM12, Sherwood and Illustris simulations are all in very good agreement; box sizes of $60\,h^{-1}$ comoving Mpc are large enough to effectively probe the range of column densities considered here. The same holds for the *b*-parameter distribution. In terms of the subgrid physics, when we compare a simulation with the effective star formation model of Springel & Hernquist (2003, not shown in the table) with the QUICKLYA HM runs, we find that the CDDF and *b*-parameter distributions are in

good agreement: The CDDFs agree within 10 per cent in the range of $\log(N_{H I}/$cm$^{-2}) = 12.5$–14.5, while the *b*-parameter distribution agrees within 25 per cent over the whole range. Since these errors are smaller than the statistical uncertainties of the data, for our purposes, QUICKLYA does not significantly impact on the column density range considered here when compared to a more detailed star formation model. Finally, the *b*-parameter distribution from Illustris converges within 10 per cent when using S/N values in the range of 20–40 per resolution element (the reference case is 30) at 17–70 km s^{-1}, while the CDDFs agree within 0.05 dex in the range of $\log(N_{H I}/$cm$^{-2}) = 13$–14.5.

4 RESULTS

In Fig. 1 (left-hand panel), we show the main result of this work: the linewidth distributions for the simulations and COS data. It is clear that HM01 and Illustris do not provide a good fit to the data. The most problematic ranges are at $b = 25$–45 km s^{-1}, where HM01 and Illustris underpredict the number of lines by roughly a factor of 2, and below 20 km s^{-1}, where these models are a factor of 4 higher than the data. The Sherwood simulation is in better agreement with the data, although it still slightly overpredicts (underpredicts) the number of lines at < 20 km s^{-1} ($b = 40$–60 km s^{-1}). We should caution here, however, that the distribution at $b < 20$ km s^{-1} is not fully converged with mass resolution for the HM and Sherwood simulations, and will slightly underpredict the incidence of narrow lines. However, this regime is numerically converged for Illustris. The median *b*-values are 28.0, 34.5 and 36.5 km s^{-1} for HM01, HM01$_{hot}$ and HM01$_{vhot}$, respectively; 32.9 km s^{-1} for HM12$_{hot}$, and 28.3 and 33.6 km s^{-1} for Illustris and Sherwood, respectively, while the COS data have a median of 36.2 km s^{-1}.

Only the HM01$_{hot}$ and HM12$_{hot}$ simulations, which have been obtained by multiplying the He I photoheating rates by a factor of 3, are in good agreement with the data. Here HM01$_{hot}$ is around
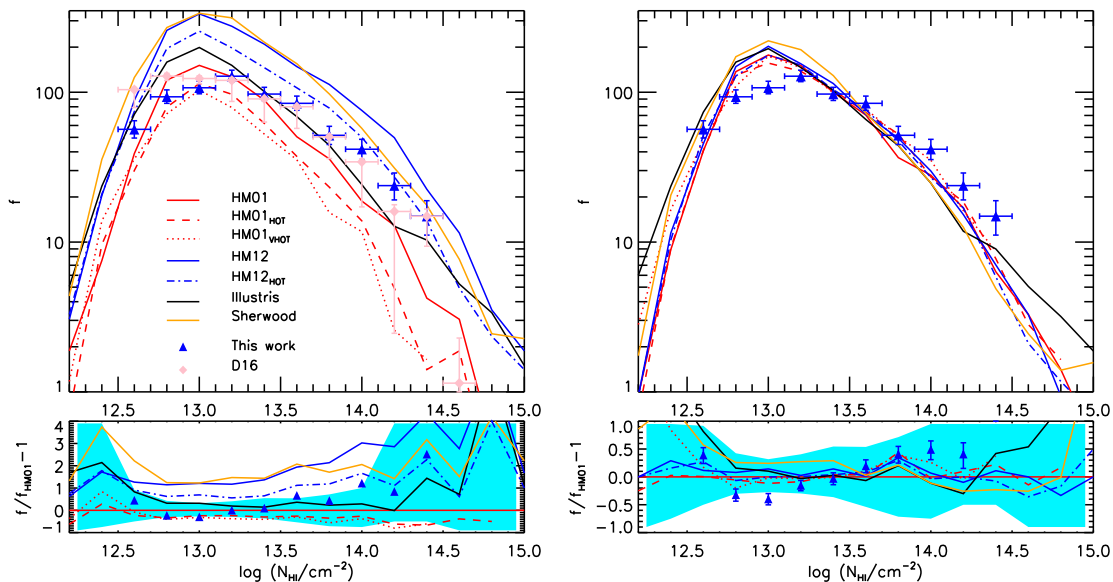
Figure 2. Left-hand panel: the corresponding CDDF (logarithmic scale) for the data described in Fig. 1 with the addition of the HM12 model (solid blue curve). No scaling has been applied to the mean transmission of the simulated spectra. Right-hand panel: the effect of scaling the optical depths (and hence H I photoionization rate) to fit the CDDF in the range of $\log(N_{\mathrm{H_I}}/\mathrm{cm}^{-2}) = 13$–$14$. Data are affected by incompleteness at $\log(N_{\mathrm{H_I}}/\mathrm{cm}^{-2}) \leq 13$.

17 000 K (4000 K) hotter than HM01 at $z = 0.1$ for overdensities $\delta = 4$–40 ($\delta = 0$). For the corresponding HM12 simulation, the change in temperature is similar. HM01$_{\mathrm{vhot}}$, in which the He II photoheating rate has been increased by a factor of 5, is instead too hot and underpredicts the number of narrow lines with $b < 25\,\mathrm{km\,s^{-1}}$.

Interestingly, the Illustris simulation is remarkably close to the HM01 model, despite the considerable differences in the subgrid physics used in these simulations. In the right-hand panel of Fig. 1, we show the probability distribution function (PDF) of the gas temperature for overdensities $\delta = 4$–40 – this selects systems in the column density range considered in this work (cf. Schaye 2001). The HM01 model is too cold to produce broad lines; the HM01$_{\mathrm{vhot}}$ model instead has a PDF peaking at $10^{4.35}$ K and in general more gas in the range of $10^{4.25}$–10^{5} K due to enhanced photoheating. The Sherwood run has temperatures closer to that of HM01$_{\mathrm{vhot}}$ and HM01$_{\mathrm{hot}}$ runs, although also exhibits a peak at 10^{5} K arising from galactic feedback. In contrast, the Illustris simulation shows much higher temperatures, with a PDF that peaks at $10^{6.5}$ K; this hot gas is too collisionally ionized to produce Lyα absorption, resulting in a similar b-parameter distribution to HM01. This is due to the very energetic AGN bubble injections in Illustris, which drive strong shocks that travel into the IGM and fill most of the volume at $z \sim 0.1$.

Finally, we have also analysed further simulations not presented in Fig. 1 with a wider range of feedback implementations. A Sherwood run with only stellar feedback results in an increase by roughly $3\,\mathrm{km\,s^{-1}}$ in the peak of the b-parameter distribution with respect to a QUICKLYA model, while the implementation of AGN feedback (orange solid line in Fig. 1) increases this value further by another $2\,\mathrm{km\,s^{-1}}$. Similarly, an increase of $4\,\mathrm{km\,s^{-1}}$ in the peak of the distribution was found when comparing a kinetic wind implementation with $480\,\mathrm{km\,s^{-1}}$ winds with the HM01 run. This demonstrates that the impact of stellar and AGN feedback on the IGM temperature distribution is strong, and suggests that the Lyα forest b-parameter distribution is a useful diagnostic of galactic feedback in the low-redshift Universe.

In the left-hand panel of Fig. 2, we also compare the CDDF, $f = \mathrm{d}^2 N/\mathrm{dlog}\,N_{\mathrm{H_I}}\mathrm{d}z$, of the simulations to the COS data. The HM01 and the Illustris simulations – the latter uses the Faucher-Giguère et al. (2009) UVB model – are in good agreement with the data in the range of $\log N_{\mathrm{H_I}}/\mathrm{cm}^{-2} = 13$–$14$, while the Sherwood and HM12 runs overpredict the number of absorption systems by a factor of ~ 2. The HM12$_{\mathrm{hot}}$ model results in a better agreement (since the neutral hydrogen fraction scales approximately $T^{-0.7}$ through the recombination coefficient) but still lies significantly above the data. In this comparison, there is no rescaling of optical depths, and these simulations have values of Γ and $\overline{F}$ as summarized in Table 1 (cf. $\overline{F} = 0.983$ from D16).

In the right-hand panel, we show what happens when we require the simulations to fit the CDDF in the range we consider most robust, $\log(N_{\mathrm{H_I}}/\mathrm{cm}^{-2}) = 13$–$14$, by rescaling the optical depths in the mock spectra. The values of the mean transmitted flux, $\overline{F}_{\mathrm{f}}$, and photoionization rate, Γ_{f}, inferred are listed in Table 1. Overall, we find that the mean transmitted fluxes are in the range of $\overline{F}_{\mathrm{f}} = [0.977 - 0.982]$, in good agreement with the D16 value (having verified that matching the D16 mean transmitted flux or the CDDF at these column densities is roughly equivalent), and the inferred photoionization rates are in the range of $\Gamma_{\mathrm{f}} = [0.05 - 0.1] \times 10^{-12}\,\mathrm{s^{-1}}$ (these values must be compared to the original UVB values Γ used as an input for the simulations; see Table 1). The latter are a factor of 1.5–3 higher than predicted by the widely used HM12 UVB model and are in very good agreement with recent results (Shull et al. 2015; Cristiani et al. 2016; Gaikwad et al. 2016a,b; Khaire et al. 2016). Note also that the effects of feedback appear to be more prominent for absorbers with column densities $\log(N_{\mathrm{H_I}}/\mathrm{cm}^{-2}) > 14.5$.

5 CONCLUSIONS

We have used hydrodynamic simulations to explore several properties of the Lyα forest at $z = 0.1$: the b-parameter distribution, CDDF and mean transmitted flux. The simulations probe a wide range of different UVBs, feedback and star formation implementations, box sizes and resolutions. We find that several simulations

fail in reproducing the linewidth distribution, underpredicting the number of lines with *b*-parameter values 25–45 km s^{-1} by a factor of 2 when compared to the observational data. This is either because the gas is too cold or, in models with vigorous AGN feedback, collisionally ionized. This tension is partly alleviated when considering alternative feedback models (less aggressive AGN feedback and galactic winds) used in the Sherwood run; it only disappears in an *ad hoc* model with enhanced photoheating, resulting in a median temperature 10^5 K for the IGM with overdensities $\delta = (4-40)$.

The CDDF and mean flux are furthermore reproduced only if the photoionization rate is higher than predicted by the HM12 model by at least a factor 1.5. The discrepancy between the values of the photoionization rate required to match the COS data and those predicted by the HM12 model is around a factor of 2, rather than the factor of 5 suggested by Kollmeier et al. (2014). This is largely due to the presence of hot(ter) gas in our simulations. Overall, we conclude that a comparison of models to the observed *b*-parameter distributions provides a valuable diagnostic of feedback in the low-redshift IGM, and may help pinpoint any missing physical ingredients in current hydrodynamic simulations in the form of additional or different thermal feedback or turbulence (e.g Iapichino, Viel & Borgani 2013).

ACKNOWLEDGEMENTS

REFERENCES

Bolton J. S., Viel M., Kim T.-S., Haehnelt M. G., Carswell R. F., 2008, MNRAS, 386, 1131
Bolton J. S., Puchwein E., Sijacki D., Haehnelt M. G., Kim T.-S., Meiksin A., Regan J. A., Viel M., 2017, MNRAS, 464, 897
Carswell R. F., Webb J. K., 2014, Astrophysics Source Code Library, record ascl:1408.015
Cristiani S., Serrano L. M., Fontanot F., Vanzella E., Monaco P., 2016, MNRAS, 462, 2478
Danforth C. W. et al., 2016, ApJ, 817, 111 (D16)
Davé R., Oppenheimer B. D., Katz N., Kollmeier J. A., Weinberg D. H., 2010, MNRAS, 408, 2051
Faucher-Giguère C.-A., Lidz A., Zaldarriaga M., Hernquist L., 2009, ApJ, 703, 1416
Ford A. B., Oppenheimer B. D., Davé R., Katz N., Kollmeier J. A., Weinberg D. H., 2013, MNRAS, 432, 89
Gaikwad P., Khaire V., Choudhury T. R., Srianand R., 2016, MNRAS, 466, 838
Gaikwad P., Srianand R., Choudhury T. R., Khaire V., 2016, preprint (arXiv:1610.06572)
Gurvich A., Burkhart B., Bird S., 2016, preprint (arXiv:1608.03293)
Haardt F., Madau P., 2001, preprint (astro-ph/0106018) (HM01)
Haardt F., Madau P., 2012, ApJ, 746, 125 (HM12)
Hinshaw G., Larson D., Komatsu E. et al., 2013, ApJS, 208, 19
Iapichino L., Viel M., Borgani S., 2013, MNRAS, 432, 2529
Janknecht E., Reimers D., Lopez S., Tytler D., 2006, A&A, 458, 427
Khaire V., Srianand R., 2015, MNRAS, 451, L30
Khaire V., Srianand R., Choudhury T. R., Gaikwad P., 2016, MNRAS, 457, 4051
Kim T.-S., Partl A. M., Carswell R. F., Müller V., 2013, A&A, 552, A77
Kirkman D., Tytler D., Lubin D., Charlton J., 2007, MNRAS, 376, 1227
Kollmeier J. A. et al., 2014, ApJ, 789, L32
Kriss G. A., 2011, COS Instrument Science Report 2011-01: Improved Medium Resolution Line Spread Functions for COS FUV Spectra. STScI, Baltimore, MD
Nelson D. et al., 2015, Astron. Comput., 13, 12
Pachat S., Narayanan A., Muzahid S., Khaire V., Srianand R., Wakker B. P., Savage B. D., 2016, MNRAS, 458, 733
Planck Collaboration XVI, 2014, A&A, 571, A16
Puchwein E., Springel V., 2013, MNRAS, 428, 2966
Rahmati A., Schaye J., Crain R. A., Oppenheimer B. D., Schaller M., Theuns T., 2016, MNRAS, 459, 310
Savage B. D., Kim T.-S., Wakker B. P., Keeney B., Shull J. M., Stocke J. T., Green J. C., 2014, ApJS, 212, 8
Schaye J., 2001, ApJ, 559, 507
Shull J. M., Danforth C. W., Tilton E. M., 2014, ApJ, 796, 49
Shull J. M., Moloney J., Danforth C. W., Tilton E. M., 2015, ApJ, 811, 3
Sijacki D., Springel V., Di Matteo T., Hernquist L., 2007, MNRAS, 380, 877
Springel V., 2005, MNRAS, 364, 1105
Springel V., 2010, MNRAS, 401, 791
Springel V., Hernquist L., 2003, MNRAS, 339, 289
Tepper-García T., Richter P., Schaye J., Booth C. M., Dalla Vecchia C., Theuns T., 2012, MNRAS, 425, 1640
Tornatore L., Borgani S., Viel M., Springel V., 2010, MNRAS, 402, 1911
Viel M., Haehnelt M. G., Springel V., 2004, MNRAS, 354, 684
Villaescusa-Navarro F. et al., 2016, MNRAS, 456, 3553
Vogelsberger M., Genel S., Sijacki D., Torrey P., Springel V., Hernquist L., 2013, MNRAS, 436, 3031
Vogelsberger M. et al., 2014, Nature, 509, 177
Wakker B. P., Hernandez A. K., French D. M., Kim T.-S., Oppenheimer B. D., Savage B. D., 2015, ApJ, 814, 40
Werk J. K. et al., 2016, ApJ, 833, 54
Weymann R. J. et al., 1998, ApJ, 506, 1

This paper has been typeset from a TeX/LaTeX file prepared by the author.